SUPPORTING INFORMATION

Structural Insights of Li^+ Doped $P\bar{6}$ Crystals of Upconverting $NaYF_4:Yb^{3+}/M^{3+}$ ($M^{3+}=Er^{3+}$ or Tm^{3+}) through Extensive Synchrotron Radiation-based X-Ray Probing

Preeti Verma[a], Debasish Sarkar[b,c], Parasmani Rajput[d], Manvendra Narayan Singh[e], Rajendra Sharma[f] and Supratim Giri[*,a,c]*

[a]Department of Chemistry, National Institute of Technology, Rourkela, 769008, India

[b]Department of Ceramic Engineering, National Institute of Technology, Rourkela, 769008, India

[c]Centre for Nanomaterials, National Institute of Technology, Rourkela, 769008, India

[d]Beamline Development and Application Section, Bhabha Atomic Research Centre Trombay, Mumbai-400085, India

[e]Hard X-ray Applications Lab, Synchrotrons Utilization Section, Raja Ramanna Centre for Advanced Technology, Indore - 452013, India

[f]Technical Physics Division, Bhabha Atomic Research Centre, Trombay Mumbai-400085, India

Table S1: Elemental analysis by ICP-OES measurement.

Nominal Li^+ (mol%)	EL series ICP-OES (mol%)	TL series ICP-OES (mol%)
10	1.57	0.3
30	5.07	3.31
50	7.76	9.42
80	13.11	13.12
100	20.07	21.01

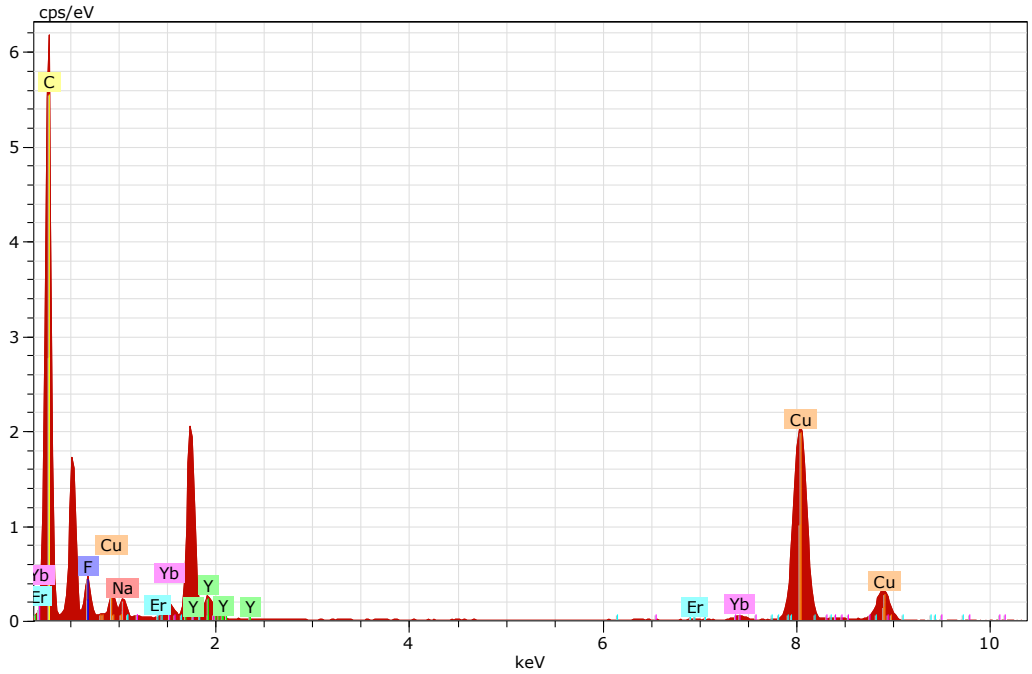

Figure S1: EDAX spectra of EL-0.

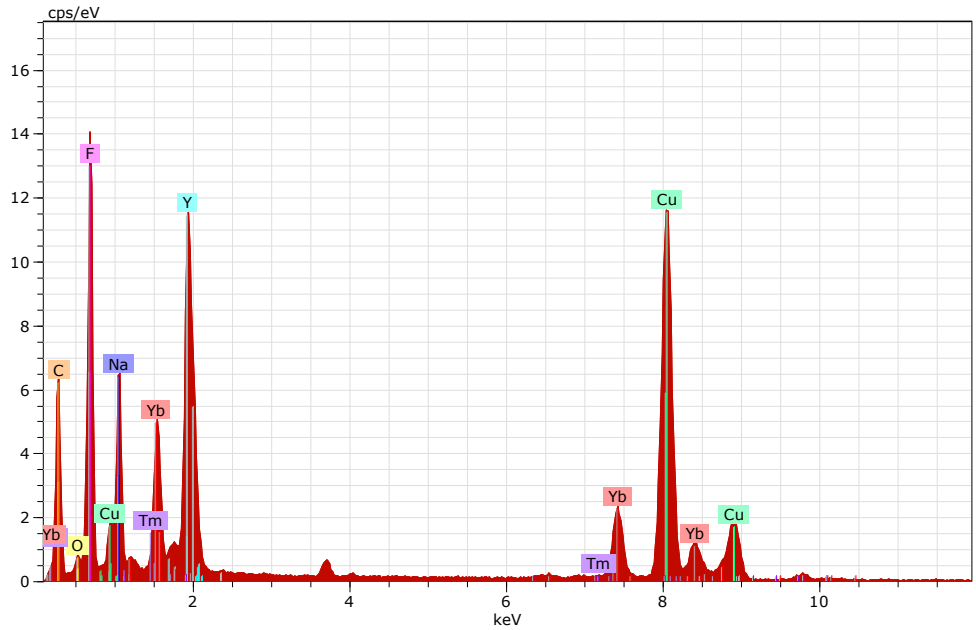

Figure S2: EDAX spectra of TL-0.

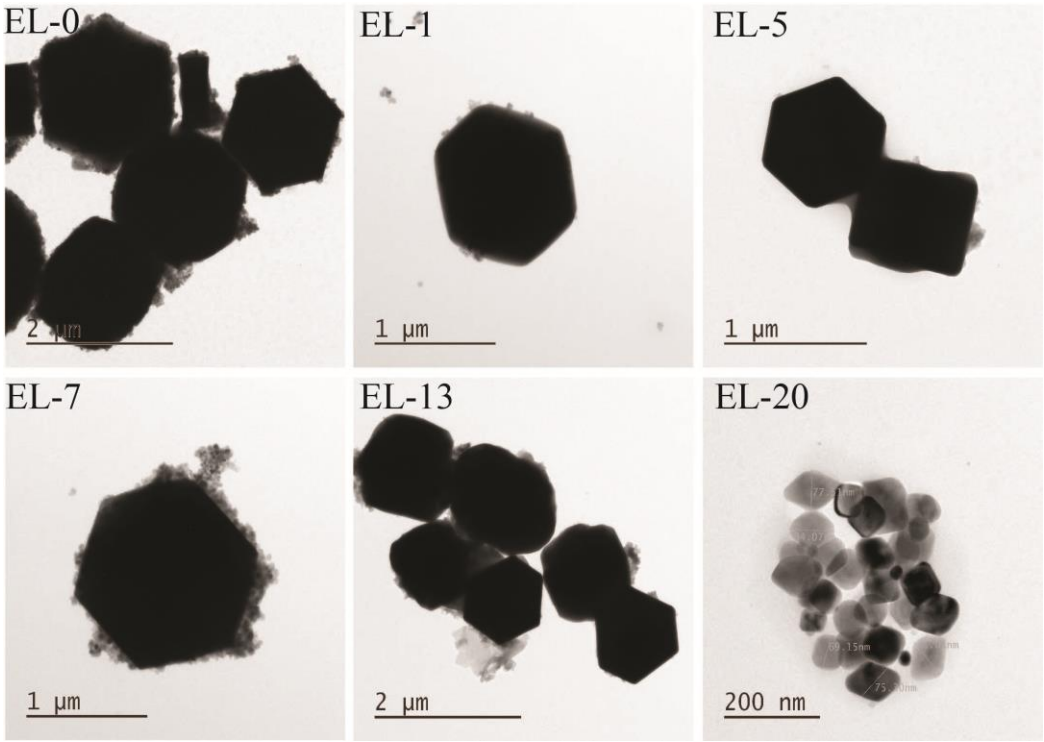

Figure S3: Bright field TEM images of different samples from EL series.

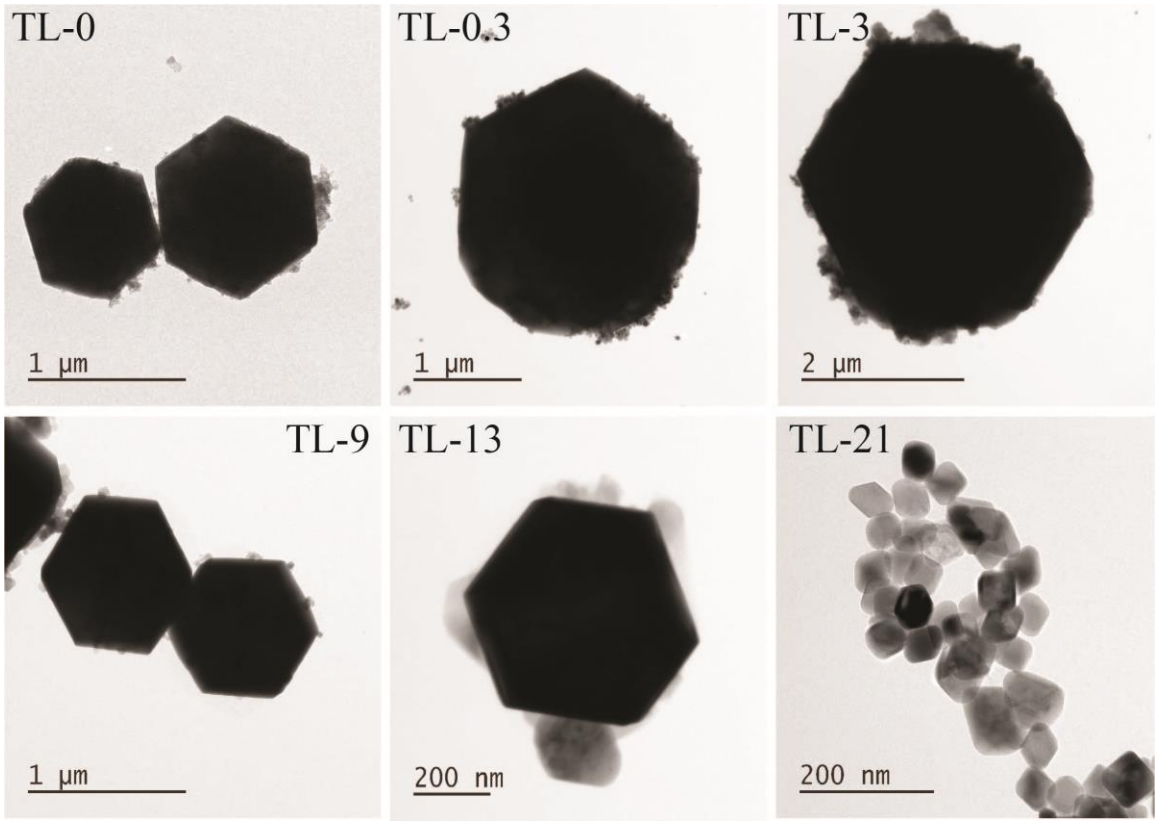

Figure S4: Bright field TEM images of different samples from TL series.

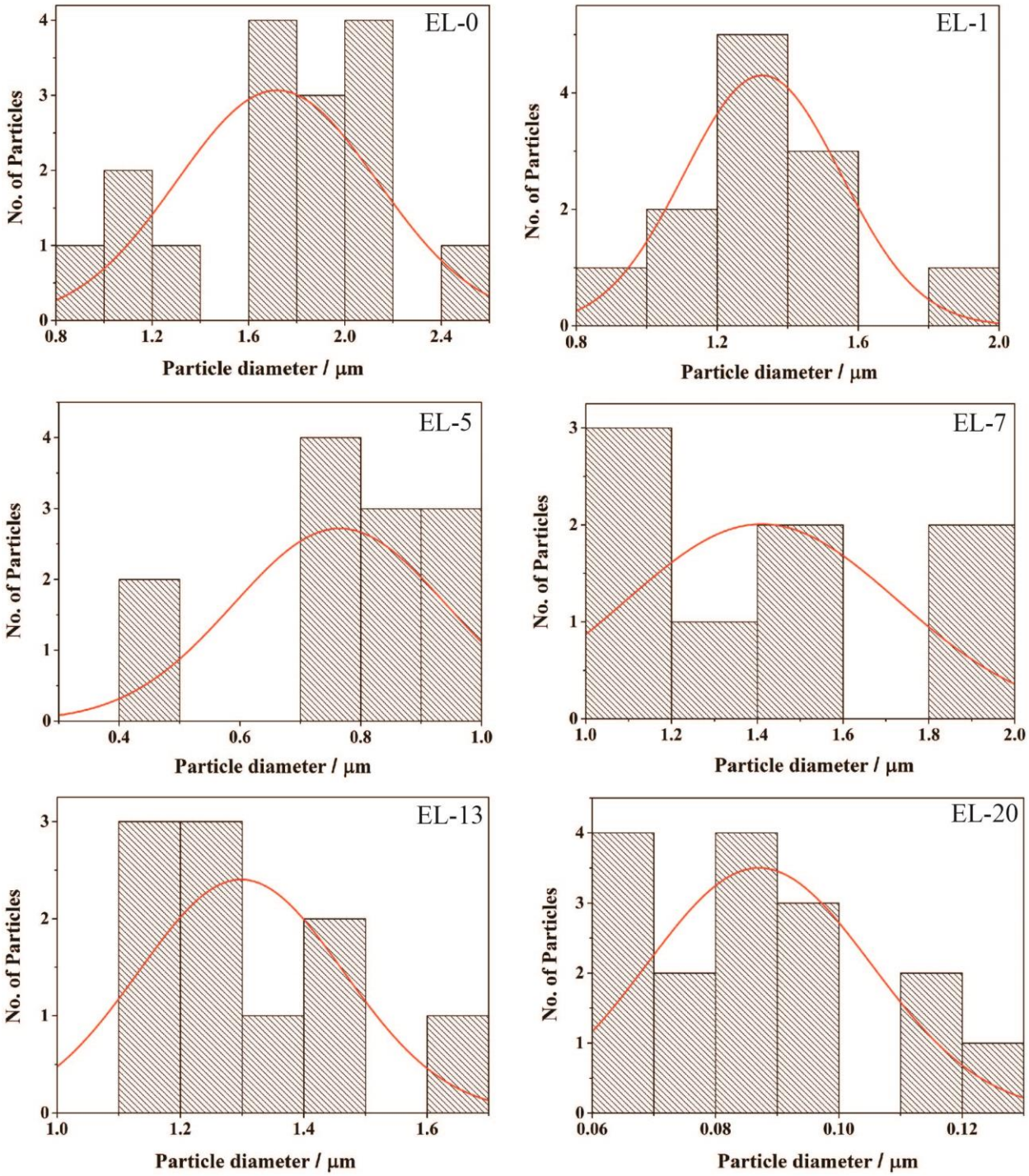

Figure S5: The average particle size distribution of different samples from EL series.

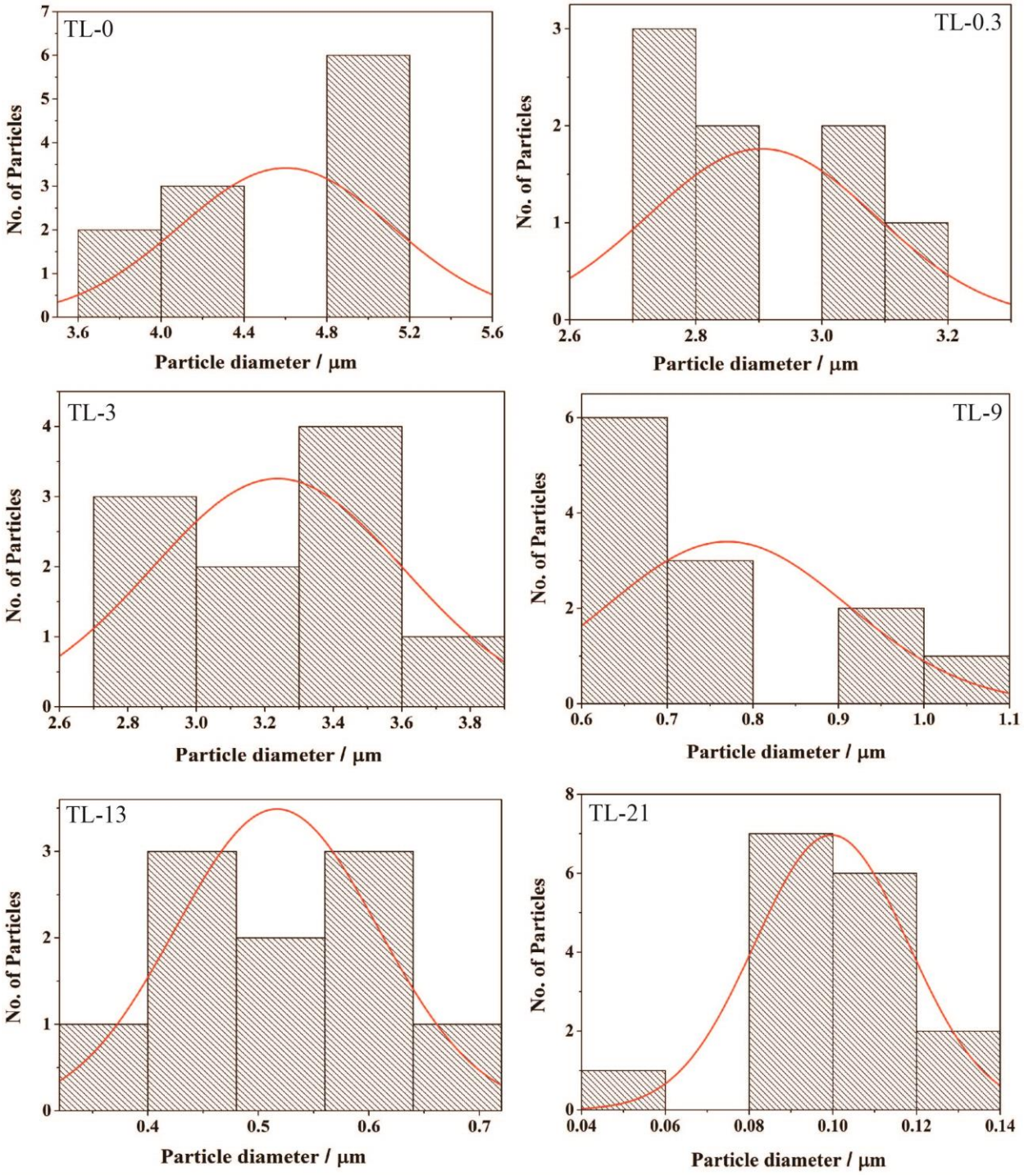

Figure S6: The average particle size distribution of different samples from TL series.

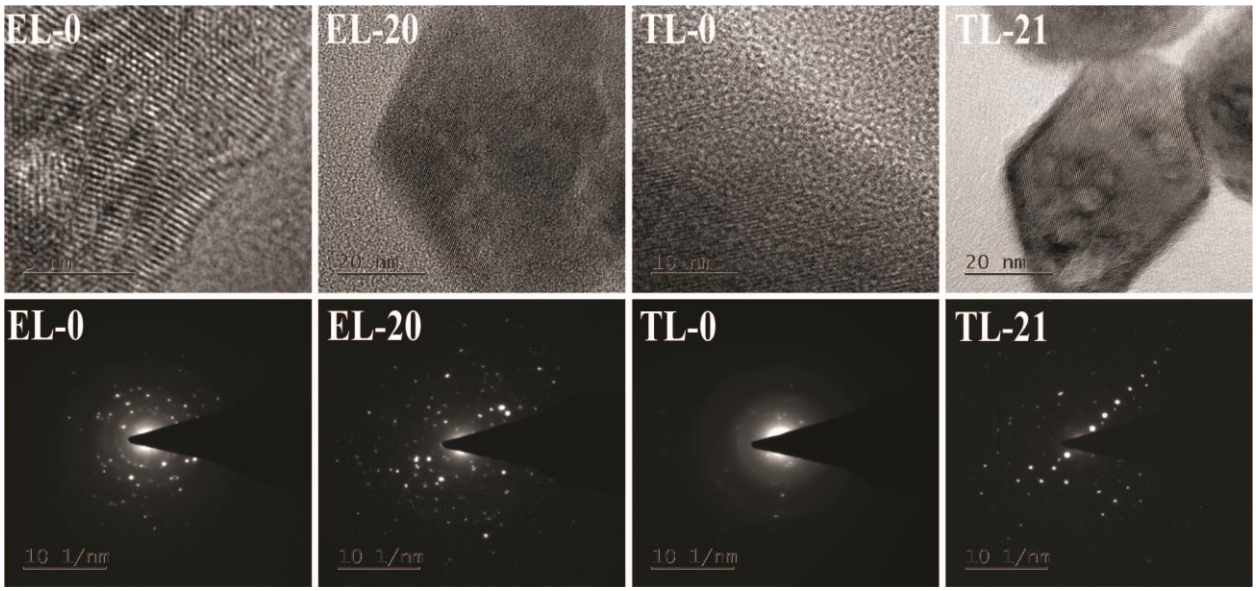

Figure S7: HRTEM and SAED pattern of selected samples from EL and TL series.

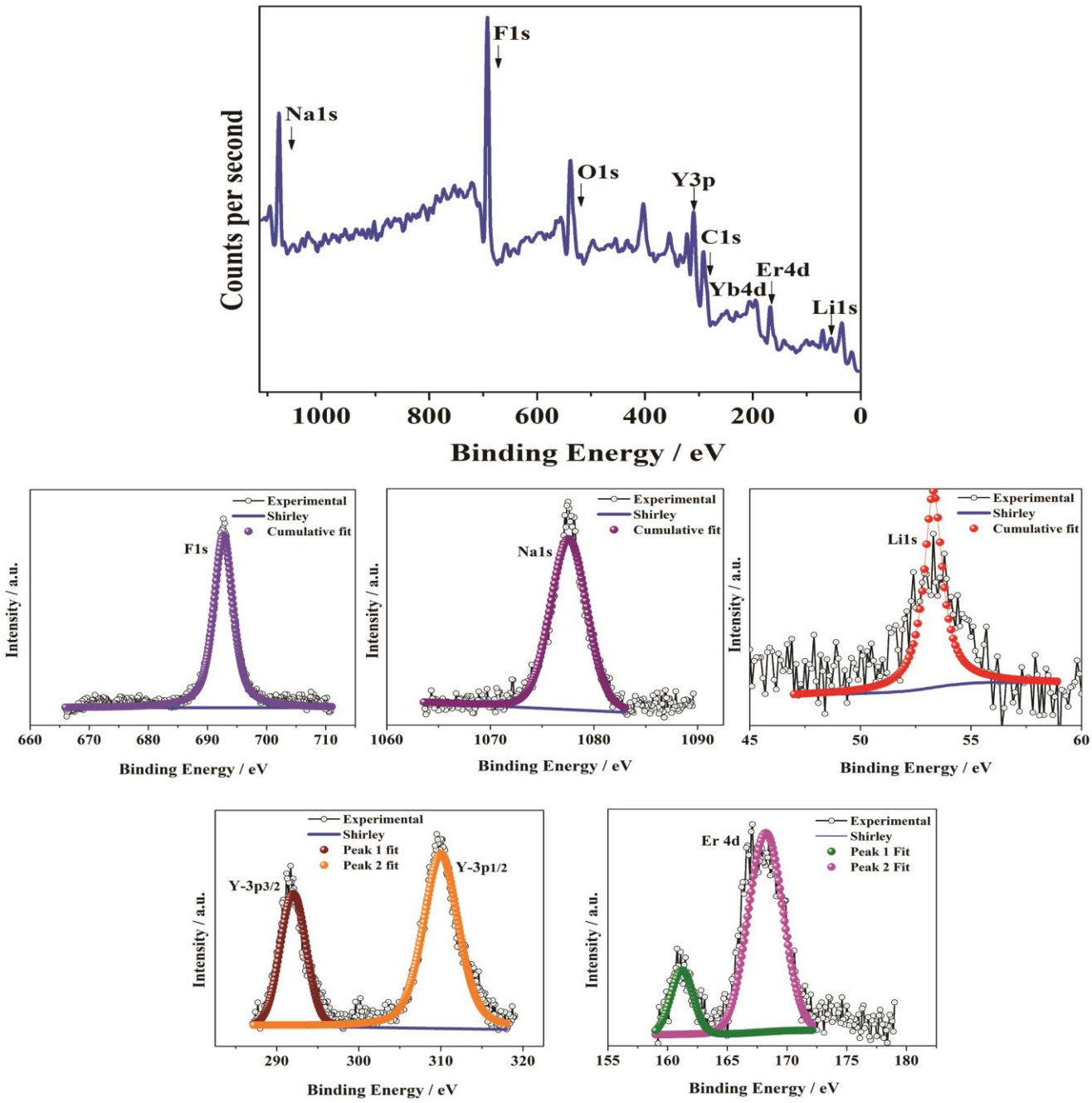

Figure S8: XPS spectra of oleic acid capped EL-5 and the cumulative peak fit of the constituent elements.

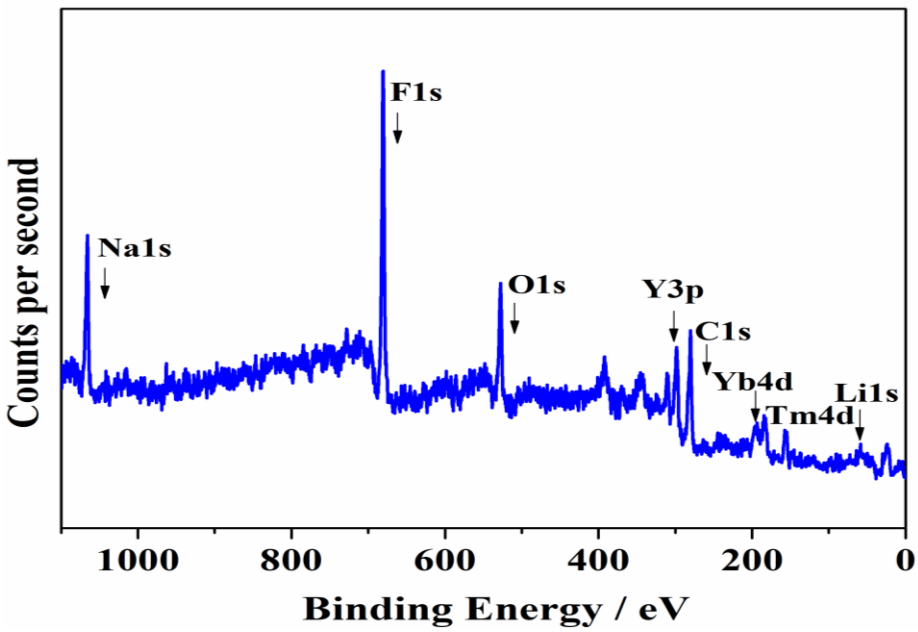

Figure S9: XPS spectra of TL-9.

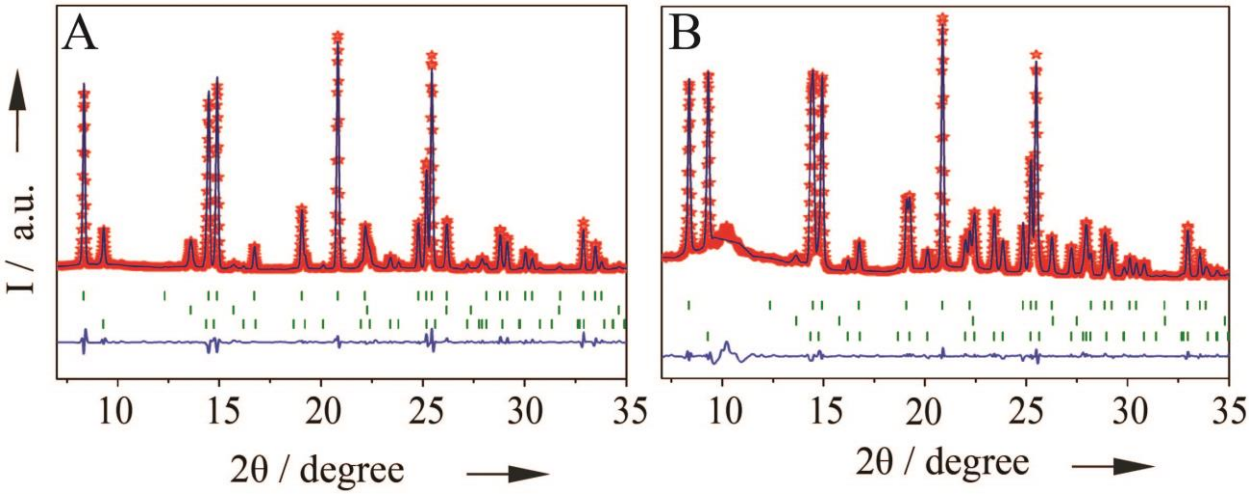

Figure S10: Rietveld refinement plots of (A) EL-1 and (B) EL-7.

Table S2: Atomic coordinates of $P\bar{6}$ space group and Interstitial void position used for Rietveld refinement.

Elements	x	y	z	Site
Y1	0.00000	0.00000	0.00000	1a
Y2	0.66667	0.33333	0.50000	1f
Na1	0.66667	0.33333	0.50000	1f
Na2	0.33333	0.66667	0.62925	2h
F1	0.61300	0.07600	0.00000	3j
F2	0.68700	0.73863	0.50000	3k

Interstitial Void Position (Tetrahedral and Octahedral)

HCP Voids	x	y	z
Tetrahedral	0.00000	0.00000	0.37500
	0.00000	0.00000	0.62500
	0.66666	0.33333	0.12500
	0.66666	0.33333	0.87500
Octahedral	0.33333	0.66666	0.25000
	0.33333	0.66666	0.75000

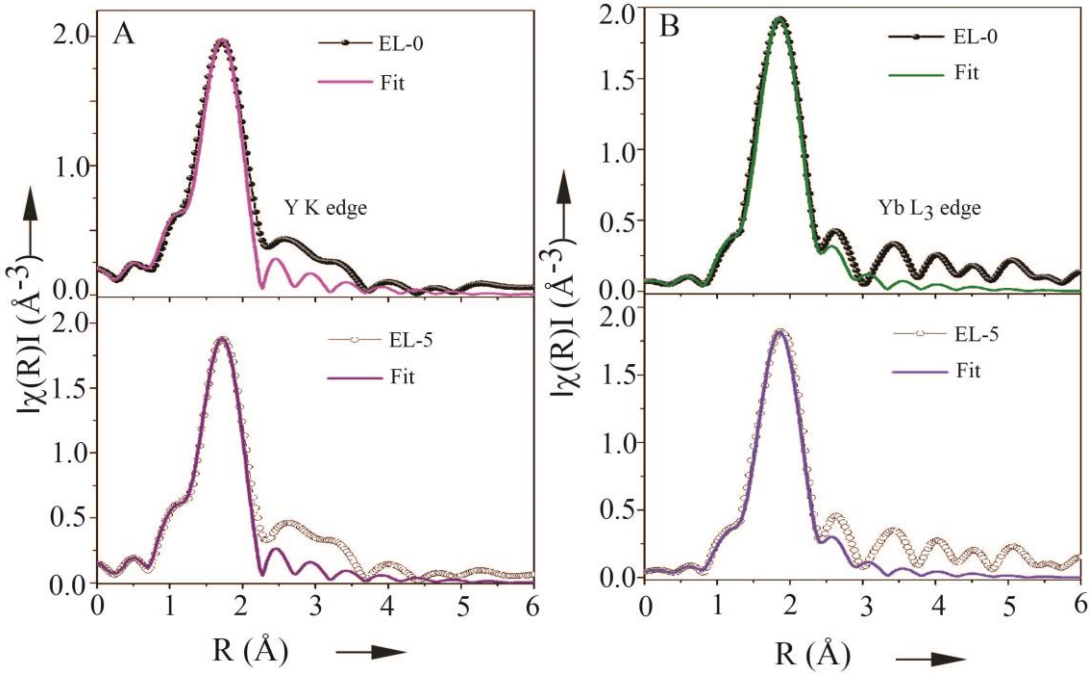

Figure S11: The Fourier Transform (FT) of k^2-weighted $\chi(k)$ spectra of EL-0 and EL-5 samples (A) at Y K and, (B) Yb L_3 edges, respectively.

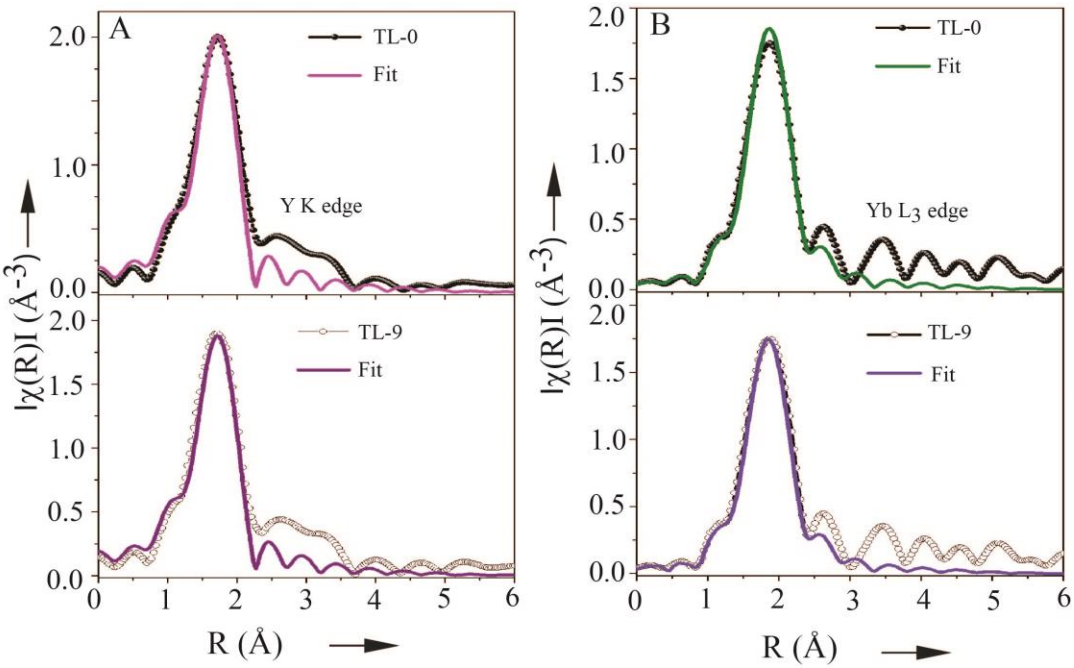

Figure S12: The Fourier Transform (FT) of k^2-weighted $\chi(k)$ spectra of TL-0 and TL-9 samples (A) at Y K and, (B) Yb L_3 edges, respectively.

Table S3: From the Er L_3, Y K and Yb L_3-edges EXAFS data fitting, we have obtained variation of CN (co-ordination number), *R* (bond distance) and σ^2 (Debye-Waller factor). The numbers in parentheses indicate the uncertainty in the last digit.

	Er L_3-edge			Y K-edge			Yb L_3-edge		
Sample	CN_{Er-F}	R_{Er-F}(Å)	σ^2_{Er-F}(Å^2)	CN_{Y-F}	R_{Y-F}(Å)	σ^2_{Y-F} (Å^2)	CN_{Yb-F}	R_{Yb-F} (Å)	σ^2_{Yb-F} (Å^2)
EL-0	9.0(2)	2.289 (3)	0.0026 (3)	8.9(2)	2.295(2)	0.0038(3)	9.0(2)	2.275(3)	0.0057(3)
EL-5	8.7(2)	2.304 (3)	0.0037(4)	8.7(3)	2.297(3)	0.0042(3)	8.7(3)	2.277(3)	0.0059(4)

Table S4: From the Tm L_3, Y K and Yb L_3-edges EXAFS data fitting, we have obtained variation of CN (co-ordination number), *R* (bond distance) and σ^2 (Debye-Waller factor). The numbers in parentheses indicate the uncertainty in the last digit.

	Tm L_3-edge			Y K-edge			Yb L_3-edge		
Sample	CN_{Tm-F}	R_{Tm-F}(Å)	σ^2_{Tm-F}(Å^2)	CN_{Y-F}	R_{Y-F}(Å)	σ^2_{Y-F} (Å^2)	CN_{Yb-F}	R_{Yb-F} (Å)	σ^2_{Yb-F} (Å^2)
TL-0	9.0(2)	2.324 (3)	0.0039(3)	8.9(2)	2.296(3)	0.0037(3)	9.0(2)	2.287(3)	0.0059(3)
TL-9	8.6(3)	2.292 (3)	0.0046(3)	8.7(3)	2.297(3)	0.0042(3)	8.6(3)	2.274(3)	0.0064(4)

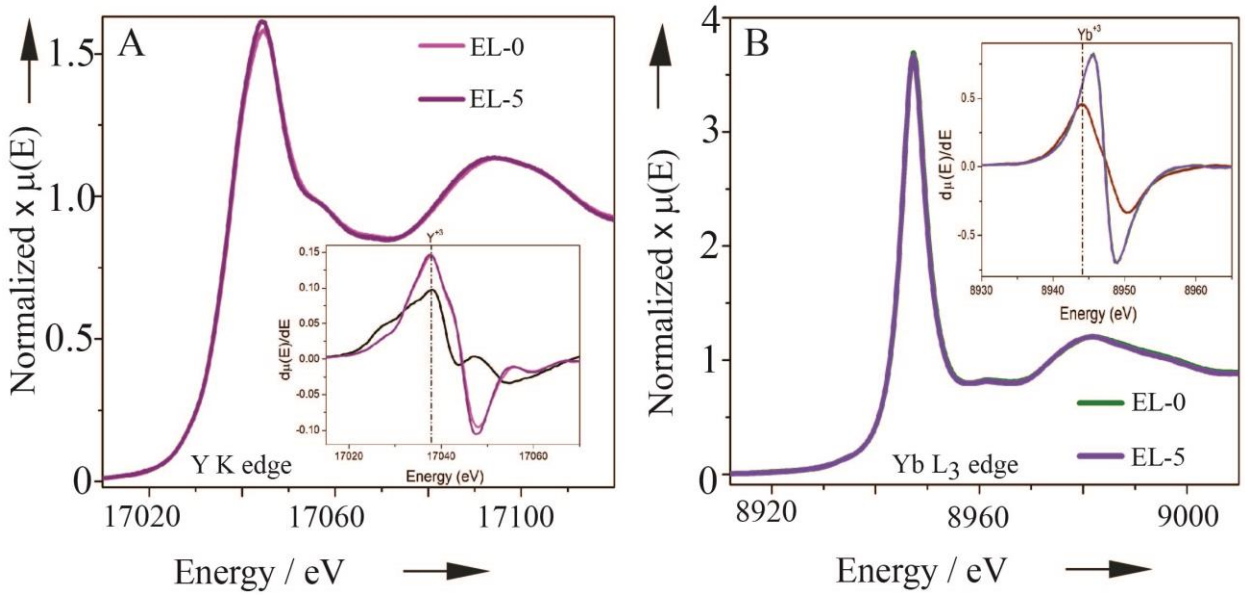

Figure S13: The normalized XANES spectra of EL-0 and EL-5 samples (A) at Y K and (B) Yb L3 edges, respectively. The inset shows 1st derivative of EL-0 and EL-5 samples along with the reference's oxide (+3 state).

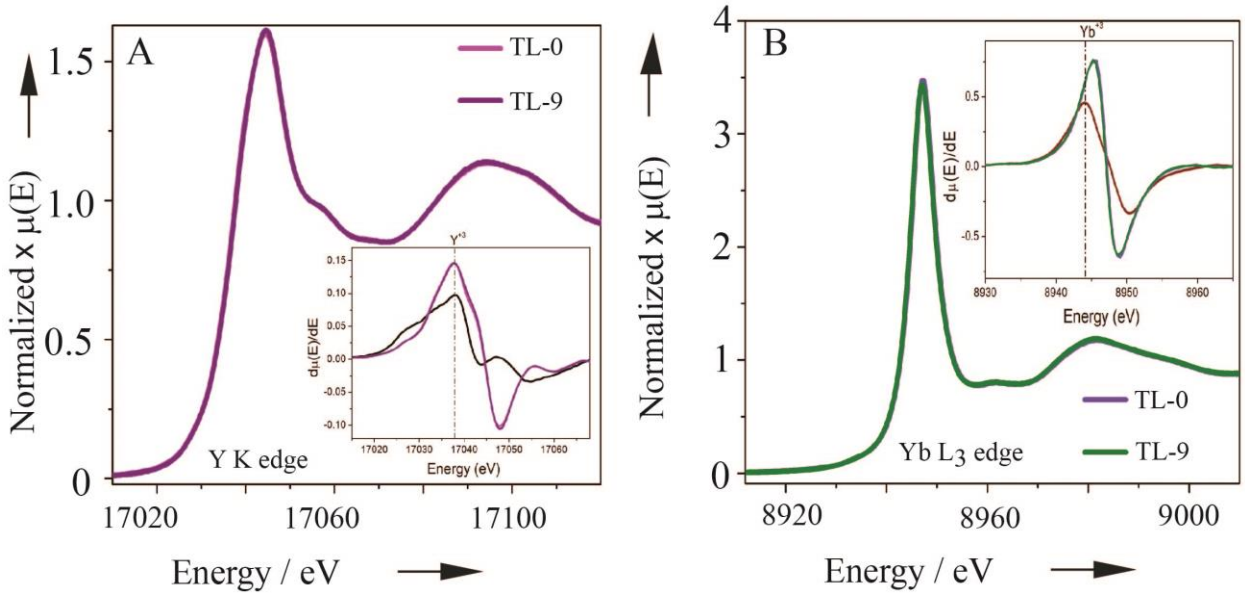

Figure S14: The normalized XANES spectra of TL-0 and TL-9 samples (A) at Y K and (B) Yb L3 edges, respectively. The inset shows 1st derivative of TL-0 and TL-9 samples along with the reference's oxide (+3 state).

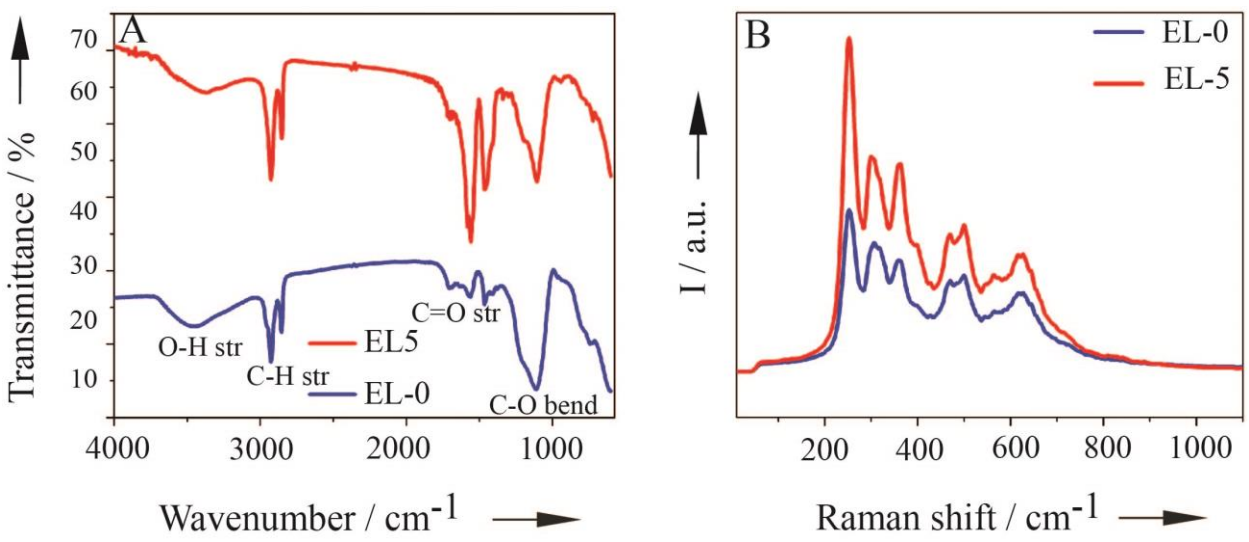

Figure S15: FTIR and Raman spectra of selected samples from EL series.

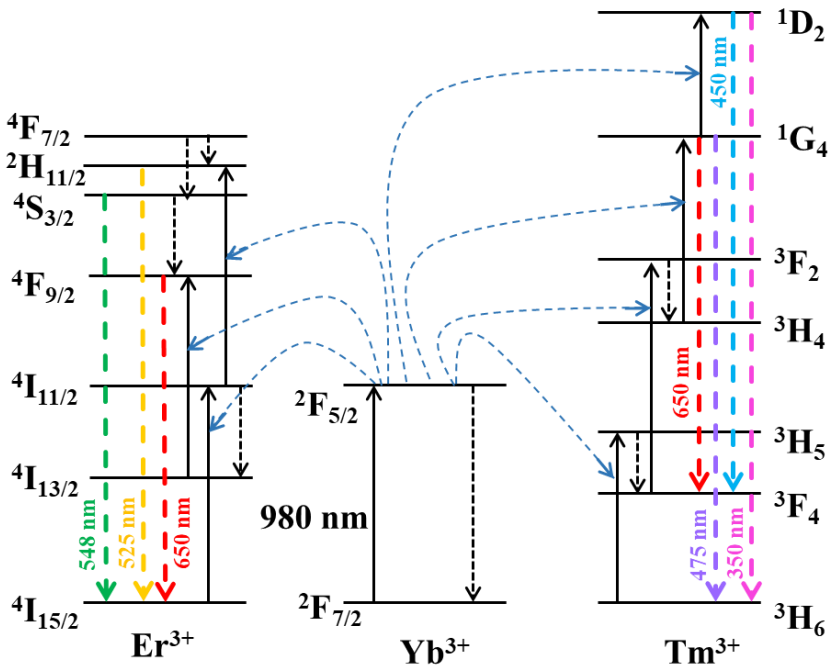

Figure S16: Proposed energy transfer mechanism for Er^{3+}, Tm^{3+} and Yb^{3+} doped crystals under 980 nm laser excitation. The plane black, blue-dashed, dashed, and coloured dashed arrows represents photon excitation, energy transfer, multiphonon relaxation, and emission processes, respectively.

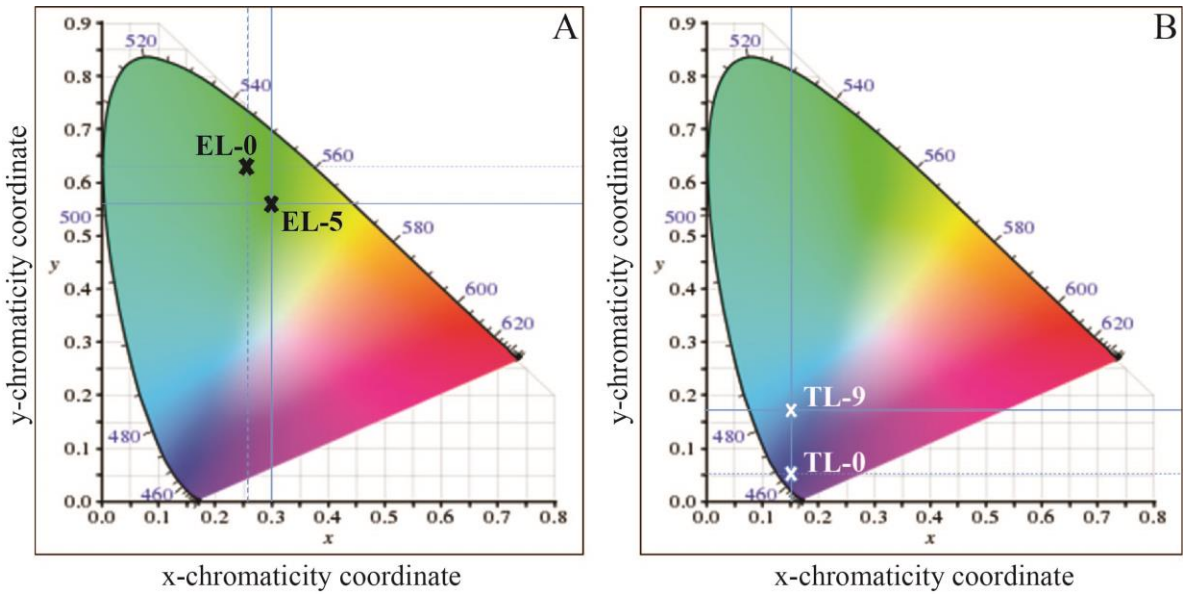

Figure S17: CIE plots of Li^+-free and Li^+-incorporated samples from (A) EL and (B) TL series.

Table S5: Strain values for different samples of EL and TL series obtained from Williamson-Hall analysis.

Sample	Strain (-10^{-4})	Sample	Strain (-10^{-4})
EL-1	8.257	TL-3	29.6
EL-5	3.701	TL-9	4.359
EL-7	39.90	TL-13	20.0

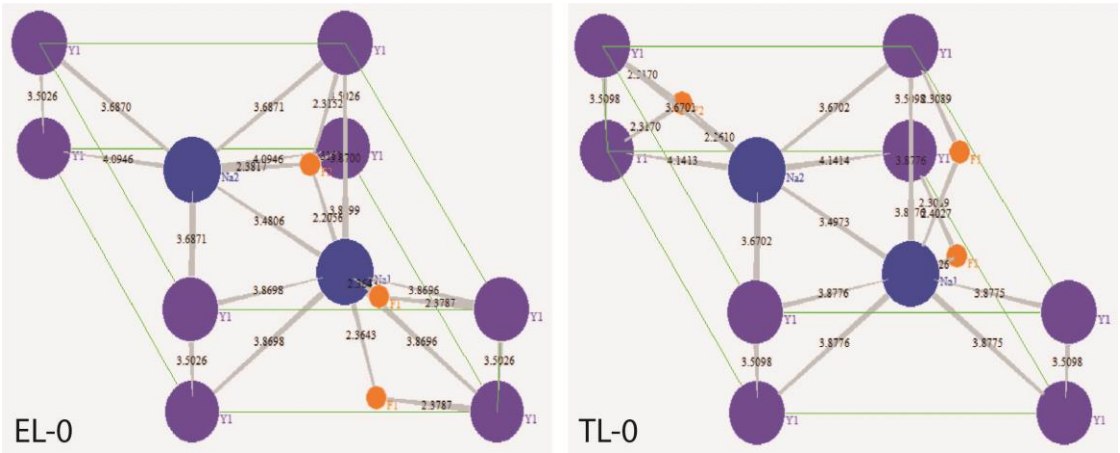

Figure S18: Crystal structures of EL-0 and TL-0 along with bond distances obtained using Powder Cell software.

Table S6: Bond distances and bond angles between different atoms in the crystal structure of samples from EL series.

Sample	*Y1-Na1 (Å)	Y1-F1 (Å)	Na2-Y1-F2 (º)	Na2-Y1-Na1 (º)
EL-0	3.8698	2.3787	29.7937	54.7852
EL-1	3.8815	2.328	25.8903	51.5834
EL-5	3.8745	2.3614	25.5095	51.6996
EL-7	3.8729	2.2765	34.7643	51.6558
EL-13	3.8734	2.4143	37.5627	51.634

***Yb^{3+}/RE^{3+} occupies the same position as Y1

Table S7: Bond distances and bond angles between different atoms in the crystal structure of samples from TL series.

Sample	*Y1-Na1 (Å)	Y1-F1 (Å)	Na2-Y1-F2 (º)	Na2-Y1-Na1 (º)
TL-0	3.8776	2.3089	36.191	51.5858
TL-0.3	3.8702	2.258	32.8517	51.8006
TL-3	3.8815	2.4688	25.7563	51.4274
TL-9	3.8753	2.371	35.687	51.7424
EL-13	3.8763	2.3412	35.0301	51.9103

***Yb^{3+}/RE^{3+} occupies the same position as Y1

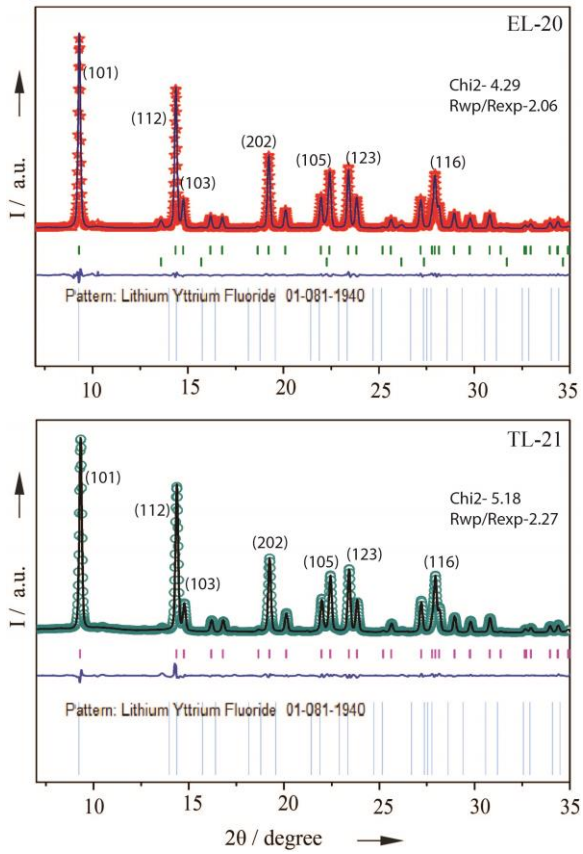

Figure S19: Rietveld refinement plots of EL-20 and TL-21

EL-20

```
-----------------------------------------------------
BRAGG R-Factors and weight fractions for Pattern #  1
-----------------------------------------------------

=> Phase:  1     Tetragonal-LiYF4
=> Bragg R-factor:   1.27       Vol:  286.001( 0.010)  Fract(%):   99.37( 0.23)
=> Rf-factor=  1.34             ATZ:         859.285   Brindley:  1.0000

=> Phase:  2     Cubic-LiF
=> Bragg R-factor:   24.6       Vol:  168.352( 0.026)  Fract(%):    0.63( 0.01)
=> Rf-factor=  25.3             ATZ:        1030.486   Brindley:  1.0000
```

TL-21

```
-----------------------------------------------------
BRAGG R-Factors and weight fractions for Pattern #  1
-----------------------------------------------------

=> Phase:  1     Tetragonal-LiYF4
=> Bragg R-factor:   1.90       Vol:  285.822( 0.014)  Fract(%):  100.00( 0.29)
=> Rf-factor=  1.69             ATZ:         837.388   Brindley:  1.0000
```

Figure S20: Refinement details of EL-20 and TL-21

Table S8. Electron density distribution in EL-0

Atoms	x/a	y/b	z/c	Electron Density ($e/Å^3$)
Y1	0.0000	0.0000	0.0000	55.9304
Na1	0.6661	0.3330	0.4998	34.8023
F1	0.6289	0.0562	0.0038	8.7489
Na2	0.3328	0.6652	0.4984	9.7953
F2	0.2654	0.0089	0.4970	7.1368

Table S9. Electron density distribution in EL-5

Atoms	x/a	y/b	z/c	Electron Density ($e/Å^3$)
Y1	0.0000	0.0000	0.0000	29.1694
Na1	0.6658	0.3332	0.4994	20.7218
F1	0.6379	0.1101	0.0022	4.1288
Na2	0.3327	0.6648	0.2909	3.3248
F2	0.0172	0.2455	0.4973	4.6415